

# Hydroxyapatite Coating On Stainless Steel Aisi 316l For Biocompatibility Application

Touheed Alam

Orcid ID: 0000-0003-4666-434X

<sup>#</sup>Department of Metallurgical Engineering, NED University of Engineering and Technology, Karachi, Pakistan.

<sup>1</sup>Email: [touheedalam.official@gmail.com](mailto:touheedalam.official@gmail.com)

**Abstract**— This paper presents the synthesis of hydroxyapatite (HAp) using eggshell biowaste and electrophoretic deposition of the material on AISI 316L stainless steel to make it more biocompatible in implantation. HAp powder was synthesized through a hydrothermal reaction and was characterized using X-ray diffraction, which proved that it was pure in terms of phase. The uniform coatings were deposited at 72 V 30-45 min after which they were sintered in an argon atmosphere. The coating was very adhesive and the critical load of the scratch test was 125 N. Simulated body fluid in vitro testing revealed that there was a slight change in pH (7.4 to 7.5) over 10 days, which implies the chemical stability of the material and proper corrosion protection. These findings show that HAp-coated 316L stainless steel is a promising and cost-effective biomaterial to use as orthopedic and dental implants because it integrates the bioactivity of hydroxyapatite and the mechanical strength of the metal.

**Keywords**— Biocompatibility applications, hydroxyapatite (Hap), AISI 316L

## 1. INTRODUCTION

Medical science has been progressing more and more on the basis of metallic implants to replace and support the damaged bone tissue. Medical implants made of metallic materials can be traced back to the 19<sup>th</sup> century, but the advancement occurred dramatically after the adoption of Lister aseptic surgical practices in the 1860s [1]. Metals have since been crucial in orthopedic surgery in both temporary implants such as screws and plates, and permanent implants such as total joint replacement [2].

Stainless Steel 316L is a popular metallic biomaterial because it combines mechanical properties, resistance to corrosion, and cost-effectiveness well in comparison to other metallic biomaterials such as titanium [23, 25]. It is popular in surgical practices due to its low carbon content and absence of inclusions. Nevertheless, human body is a very hostile, chlorine-containing, and acidic environment [31]. Although SS 316L has corrosion resistance intrinsic to it, it remains

susceptible to localized corrosion, including pitting and crevice corrosion, when implanted [14]. This corrosion results in the release of potentially toxic metal ions such as nickel, chromium and cobalt in the surrounding tissues, which may cause adverse reactions such as toxicity, allergy and even carcinogenicity [14, 15]. This is especially a problem in younger patients who can be subjected to these ions over a long period of time.

One of the most popular methods of reducing this issue is to coating the metal surface with a bioactive and biocompatible coating. The perfect candidate in this regard is hydroxyapatite (HAp) whose chemical formula is  $\text{Ca}_{10}(\text{PO}_4)_6(\text{OH})_2$ . It is the main inorganic component of natural bone and teeth and has a high level of biocompatibility, osteoconductivity, and a direct chemical bond with bone tissue [1, 2-4]. Nonetheless, HAp ceramics by themselves have low mechanical strength and are not suitable to be used in load-bearing applications. Thus, the bioactivity of the ceramic is coupled with the mechanical integrity of the metallic substrate such as SS 316L to avoid direct contact between the metal and the corrosive body fluids and to enhance bone formation and integration of the implant [6, 50].

This project will attempt to prepare HAp powder using a sustainable and cost-effective bio-waste material (eggshells) and use it as a coating on SS 316L substrates through Electrophoretic Deposition (EPD). The coated samples will be characterized to determine the phase composition, adhesion strength and in-vitro biocompatibility.

## 2. MATERIAL AND METHOD

## 2.1. Materials

Hen eggshells were taken at the local bakeries and kitchens and AISI 316L stainless steel sheets were used as the main materials. The chemicals were tri-calcium phosphate (TCP), acetone, ethanol, hydrochloric acid (HCl), and Simulated Body Fluid (SBF) preparation reagents: NaCl, NaHCO<sub>3</sub>, KCl, Na<sub>2</sub>HPO<sub>4</sub>, MgCl<sub>2</sub>·6H<sub>2</sub>O, CaCl<sub>2</sub>·H<sub>2</sub>O, Na<sub>2</sub>SO<sub>4</sub>, and tris-hydroxymethyl aminomethane ((CH<sub>2</sub>OH)<sub>3</sub>CNH<sub>2</sub>). Figure 1 shows the collected hen eggshells used as the raw calcium source for hydroxyapatite synthesis.



Figure 1 Collection of eggshells

## 2.2. Synthesis of Hydroxyapatite from Eggshells

Hydroxyapatite (HAp) was synthesized from hen eggshells collected from local sources. The eggshells were cleaned by boiling in distilled water to remove membranes, dried, and ground into a fine powder. The powder was calcined in a box furnace using a three-stage thermal treatment: heating to 450 °C for 2 h, then to 600 °C for 2 h, and finally to 900 °C for 1 h, converting calcium carbonate to calcium oxide (CaCO<sub>3</sub> → CaO + CO<sub>2</sub>). The resulting CaO was hydrated with distilled water at 90 °C to form calcium hydroxide (CaO + H<sub>2</sub>O → Ca(OH)<sub>2</sub>). This Ca(OH)<sub>2</sub> was then mixed with tri-calcium phosphate (TCP) in a 1:3 weight ratio (75 g Ca(OH)<sub>2</sub> : 225 g TCP) in distilled water. The slurry was stirred on a magnetic stirrer at 70 °C for 90 min and aged for 24 h to complete the reaction (3Ca<sub>3</sub>(PO<sub>4</sub>)<sub>2</sub> + Ca(OH)<sub>2</sub> → Ca<sub>10</sub>(PO<sub>4</sub>)<sub>6</sub>(OH)<sub>2</sub>). The mixture was filtered, and the solid residue was sintered at 900 °C for 2 h to obtain phase-pure HAp, which was finally ground into a

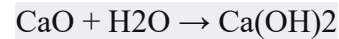
fine powder for coating applications as shown in Figure 2



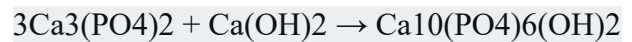
Figure 2 Hydroxyapatite from Eggshells



The resulting CaO was hydrated with distilled water at 90 °C to form calcium hydroxide



The Ca(OH)<sub>2</sub> was then mixed with tri-calcium phosphate in a stoichiometric ratio of 1:3 by weight (75g Ca(OH)<sub>2</sub> to 225g TCP) in distilled water. The slurry was stirred on a magnetic stirrer at 70 °C for 90 minutes and then aged for 24 hours. The expected reaction was



The aged mixture was filtered and the solid residue was sintered at 900 °C for 2 hours to remove any remaining water and crystallize the HAp. The final product was ground into a fine powder and characterized using XRD.

## 2.3. Substrate Preparation

Stainless Steel 316L plates were cut into samples of approximately 1 cm<sup>2</sup> area. For metallographic observation, samples were ground using SiC emery paper from 60 to 1000 grit, polished with an alumina suspension, and etched with aqua regia. For coating, all samples were ultrasonically cleaned in acetone at 50 °C for 25 minutes to remove contaminants. To create a rougher surface for better mechanical interlocking of the coating, the cleaned samples were then immersed in a dilute HCl solution for 7 hours, followed by a distilled water rinse and drying. Figure 3 showing the stainless steel substrate

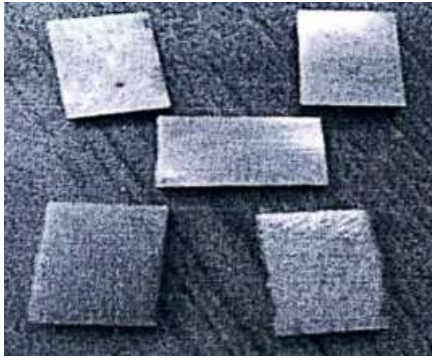


Figure 3 Stainless Steel Substrate

## 2.4. Electrophoretic Deposition (EPD) of HAp Coating

A 1 wt% stable suspension for EPD was prepared by dispersing 6g of the synthesized HAp powder in 600 ml of ethanol. A small amount of sodium dodecyl sulphate was added as a wetting agent. The EPD setup consisted of a 500 ml glass beaker, a graphite rod as the anode (+), and the prepared SS 316L sample as the cathode (-), positioned 2 cm apart. Deposition was carried out at a constant DC voltage of 72V for varying times (15, 30, 45, and 60 minutes) to achieve different coating thicknesses. After deposition, the coated samples were carefully removed and dried in air as shown in Figure 4



Figure 4 Setup of EDP

## 2.5. Sintering of Coated Samples

The green coatings were sintered in a tube furnace under an inert Argon atmosphere to prevent oxidation of the steel substrate. The sintering cycle involved heating to temperatures ranging from 200°C to 800°C with varying soaking times. After sintering, the samples were allowed to anneal in the furnace for 24 hours.

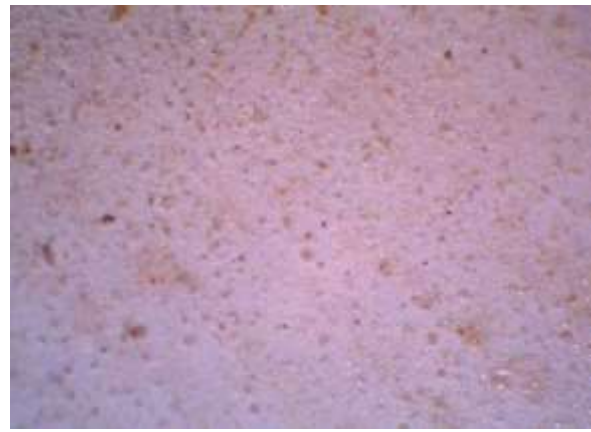


Figure 5 Coated sample after sintering

Figure 5 shows the final HAp-coated Stainless Steel 316L sample after sintering in an Argon atmosphere. The image reveals a uniform white coating layer completely covering the metal substrate with no visible cracks or delamination. This confirms that the Electrophoretic Deposition and sintering parameters were successfully optimized to produce a well-adhered, dense coating suitable for biomedical implant applications.

## 2.6. Characterization

The synthesized powder and coated samples were characterized using X-ray Diffraction (XRD) to confirm phase composition. Coating thickness and uniformity were observed using a Stereo microscope. The adhesion strength of the coating was evaluated using a scratch tester with a diamond indenter, where a load was applied until coating failure. In-vitro biocompatibility was assessed by immersing coated samples in Simulated Body Fluid (SBF) with an ionic concentration similar to human blood plasma for 10 days. The pH of the SBF was measured before and after immersion to detect any significant ion exchange.

## 3. RESULTS AND DISCUSSION

### 3.1. Hydroxyapatite Synthesis and XRD Analysis

The synthesis was multi-step and was able to convert the raw eggshells to a fine, white powder of Hydroxyapatite. Calcination of the eggshells at 900 C was effective in pushing off carbon dioxide to produce calcium oxide. The resulting hydration

generated calcium hydroxide that reacted with tricalcium phosphate to give the final HAp product. The total productivity was about 250 grams of HAp powder of 300 grams of raw eggshells, a yield of about 83 percent.

To verify the changes in the phases and purity of the end product, X-ray Diffraction analysis was conducted at key steps of the synthesis..

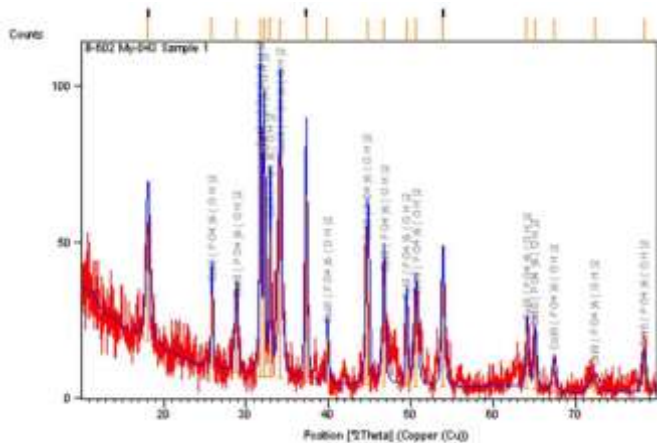
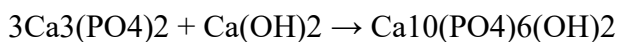


Figure 6 XRD Result of Hydroxyapatite

The XRD pattern of the final synthesized powder is shown in Figure 6. The diffraction pattern has sharp, well-defined peaks, which means that the degree of crystallinity is high. The significant peaks were noted at the 2 $\theta$  of about 25.9, 31.8, 32.2, 32.9, 34.1, 39.8, 46.7, and 49.5. These highest positions were compared with the Joint Committee on Powder Diffraction Standards (JCPDS) reference data of hydroxyapatite (JCPDS File No. 09-0432). The (002), (211), (112), (300), (202), (310), (222), and (213) planes of hexagonal HAp characteristic peaks were all located and observed to be in fine agreement with the standard pattern. This fact confirms the effective synthesis of the phase-pure hydroxyapatite through the reaction.



The fact that there were no major extraneous peaks in the final pattern that could be attributed to unreacted calcium hydroxide, calcium oxide, or tricalcium phosphate implies that the reaction had reached completion and that the sintering step at 900 o C had been adequate to produce a single-phase product that was homogeneous. The crystallinity is

also favorable in terms of coating because it is associated with long-term stability of the implant in the physiological environment.

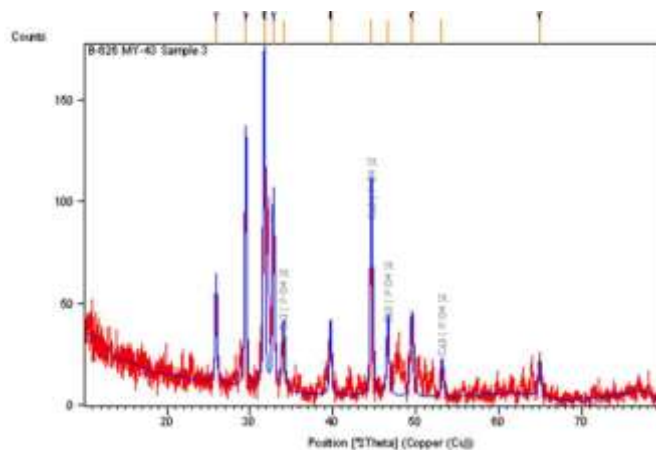


Figure 7 XRD Result of Tricalcium Phosphate

Figure 8 shows the X-ray diffraction pattern of the powder of calcium hydroxide that was obtained after the hydration of the calcined eggshells, and it indicates that the sample has strong, sharp peaks, which prove the high level of crystallinity. The characteristic peaks were located at 2 $\theta$  values of about 18.1, 28.7, 34.1, 47.1, and 50.8, which corresponded to the (001), (100), (101), (102), and (110) planes of portlandite (JCPDS card No. 04 - 0733). The fact that no residual peaks of unreacted calcium oxide (CaO) or other impurities are present means that the hydration step was done to completion. This purity and crystallinity of the Ca(OH)<sub>2</sub> intermediate is necessary in obtaining the appropriate Ca:P ratio in the next reaction with tricalcium phosphate to produce phase-pure hydroxyapatite

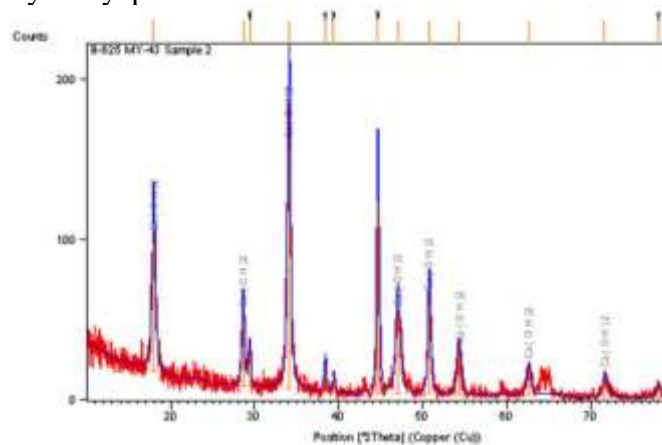


Figure 8 XRD Result of Calcium Hydroxide

Figure 8 shows the X-ray diffraction pattern of the powder of calcium hydroxide, which has been obtained after hydration of calcined eggshells. The pattern shows high and intense diffraction peaks, which prove a highly crystalline structure of portlandite. Significant peaks were observed at 2θ angles of 18.1, 28.7, 34.1, 47.1, and 50.8, which are related to the (001), (100), (101), (102), and (110) crystallographic planes, respectively, of Ca(OH)<sub>2</sub>, as expected by the Joint Committee on Powder Diffraction Standards (JCPDS) card No. 04-0733. No unreacted calcium oxide (CaO) or other impurities residual peaks were observed, which means that the hydration step (CaO + H<sub>2</sub>O → Ca(OH)<sub>2</sub>) was complete. The crystallinity and phase purity of this intermediate are essential to the formation of the appropriate stoichiometric ratio of Ca:P in the next reaction with tri-calcium phosphate to form phase-pure hydroxyapatite without the formation of unwanted secondary phases.

### 3.2. Coating Morphology and Deposition Parameters

The process parameters were found to be very critical in the quality and uniformity of the HAp coating deposited through Electrophoretic Deposition. Constant applied voltage of 72V was the main variable that affected the deposition time, which in turn affected the coating thickness and morphology. The EPD process is based on the fact that the charged HAp particles in the ethanol suspension are directed to the oppositely charged stainless steel cathode under the action of an electric field. Hamaker equation can be used to describe the deposition mass

$$m = \int \mu \cdot E \cdot C \cdot A \cdot dt$$

where m is the deposited mass, μ is the electrophoretic mobility, E is the electric field strength, C is the particle concentration, A is the deposition area, and t is the time.

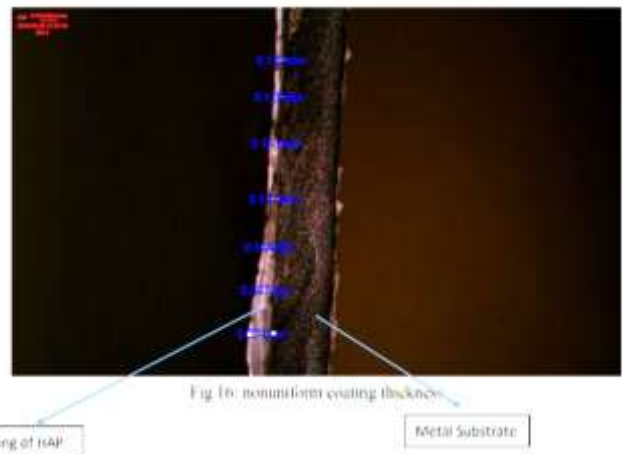


Figure 9 Nonuniform Coating Thickness

Figure 9 demonstrates a case of uneven coating. This morphology was probably caused by a lack of deposition time (15 minutes) or the suspension instability causing agglomeration of the particles. When this happens, the coating has regions of dense, uneven particle deposition and other regions of bare substrate. This non-uniformity is not desirable in the case of implant applications because it may result in the non-uniformity of bioactivity and possible weak points where corrosion may start.



Figure 10 Uniform Coating Thickness

Figure 10 shows that a uniform coating was successful and the deposition time was optimized at 30 to 45 minutes. The coating shows a uniform layer over the substrate surface having a uniform thickness. The optical micrograph is able to clearly differentiate between the dark metal substrate and the light HAp ceramic layer. This consistency is

essential to predictable in-vivo performance, where the whole surface is a predictable barrier to corrosion and a uniform surface on which the bone cells can be attached and grow. This uniformity was also aided by the acid etching pretreatment of the SS 316L surface that created micro-scale roughness that facilitates mechanical interlocking and offers a higher number of nucleation sites to the particle deposition.

### 3.3. Adhesion Strength Analysis

The bonding ability of the HAp coating and the SS 316L substrate is a critical consideration that defines the long-term performance of the implant. Lack of adhesion may result in delamination of the coating during physiological loading, exposing the underlying metal to the corrosive body environment, and producing wear debris that may result in inflammation and osteolysis.

A sintered sample was subjected to a scratch test to measure the adhesion of the coating quantitatively. During this test, a diamond stylus (Rockwell C geometry) is scanned on the coated surface under a normal load of increasing magnitude. Critical load ( $L_c$ ) at which coating failure takes place is identified by observing acoustic emission, frictional force and further microscopic examination.

Figure 10 displays an enlarged picture of the scratch track. The test showed that edge chipping was the first failure mode, which led to more severe spallation with the increase in the load. The first failure (edge chipping) critical load was measured to be 125 N.

This is a very high value and it shows that there is a very good adhesive bond between the HAp coating and the substrate of SS 316L. To compare, the coating applied to orthopedic implants is normally required to have a critical load value of more than 30 N to be able to resist surgical manipulation and physiological forces. These requirements are way below the achieved value of 125 N. Such high adhesion is explained by a number of synergistic factors.

1. **Mechanical Interlocking:** The acid etching pretreatment created a microscopically rough surface on the SS 316L substrate. During EPD and subsequent sintering, the HAp particles infiltrated these surface irregularities, creating a strong mechanical key upon densification.
2. **Sintering Under Inert Atmosphere:** Sintering the coated samples in an Argon atmosphere at temperatures up to 800°C served multiple purposes. It prevented the oxidation of the stainless steel substrate, which would have created a weak, brittle oxide layer at the interface. Simultaneously, it promoted solid-state diffusion and neck formation between individual HAp particles and between the HAp particles and the substrate surface, significantly increasing the cohesive and adhesive strength of the coating.
3. **Clean Substrate Surface:** The rigorous ultrasonic cleaning in acetone ensured the removal of all organic contaminants and oils, allowing for intimate contact between the HAp particles and the bare metal surface during deposition and sintering.

The cracks and chipping observed in Figure 10 are a direct result of the extreme localized stress from the diamond indenter and are not indicative of poor coating quality. The failure occurs within the coating or at the interface only when the applied load exceeds the practical work of adhesion, which in this case is very high

### 3.4. In-Vitro Biocompatibility and SBF Immersion Test

The primary function of the HAp coating is to impart biocompatibility and bioactivity to the otherwise bioinert SS 316L substrate. The Simulated Body Fluid (SBF) immersion test is a widely accepted in-vitro method to evaluate the bioactivity and chemical stability of a material. The SBF used in this study had an ionic composition closely matching that of human blood plasma, as detailed below in table 1

Ion	Concentration in	
	Blood (mM)	Plasma SBF (mM)
Na <sup>+</sup>	142.0	142.0

$K^+$	5.0	5.0
$Mg^{2+}$	1.5	1.5
$Ca^{2+}$	2.5	2.5
$Cl^-$	103.0	103.0
$HCO_3^-$	27.0	27.0
$HPO_4^{2-}$	1.0	1.0
$SO_4^{2-}$	0.5	0.5
pH	7.2-7.4	7.4

A coated sample was immersed in this SBF solution for a period of 10 days (240 hours) at room temperature. The pH of the solution was measured before introducing the sample and immediately after its removal at the end of the 10-day period.

The results were as follows

- **Initial pH of SBF: 7.4**
- **Final pH of SBF after 10 days: 7.5**

The negligible change in pH, an increase of only 0.1, is a highly significant finding with profound implications for biocompatibility. This stability indicates that there was no substantial dissolution or precipitation of ions from the HAp coating into the SBF solution. The following interpretations can be drawn from this result:

1. **Chemical Stability:** The HAp coating is chemically stable in a simulated physiological environment. There was no measurable release of acidic or basic ions that would alter the pH. This confirms that the sintering process produced a dense, well-crystallized HAp layer that is resistant to hydrolytic degradation.
2. **Effective Barrier Function:** The coating successfully acts as a barrier, preventing the underlying SS 316L substrate from interacting with the corrosive ions (particularly chloride ions) present in the SBF. If the coating were porous or poorly adhered, the SBF would penetrate to the substrate, leading to corrosion reactions, metal ion release, and a consequent shift in pH. The stable pH confirms that this did not occur.
3. **Non-Toxicity:** The absence of significant ion release implies that the coated implant would not leach cytotoxic ions into the

surrounding tissue in-vivo. This is a prerequisite for a material to be considered non-toxic and biocompatible [15-17].

4. **Bioactivity Potential:** While a pH change was not observed in this short-term test (which is good for stability), the stable SBF environment also provides the conditions necessary for the nucleation and growth of a bone-like apatite layer on the HAp surface over longer periods. The supersaturation of  $Ca^{2+}$  and  $PO_4^{3-}$  ions relative to apatite in the SBF, combined with a stable pH, can eventually lead to the precipitation of a new apatite layer, which is the hallmark of a bioactive material. This test confirms that the coating is capable of maintaining the delicate ionic balance required for this process.

In conclusion, the SBF immersion test provides strong evidence that the HAp-coated SS 316L samples possess the necessary chemical stability and biocompatibility for further evaluation as a candidate material for orthopedic and dental implants. The coating acts as an effective shield, preventing metal ion release while presenting a stable, bone-like surface to the biological environment.

#### 4. CONCLUSIONS

This study has been able to develop a cost-effective and sustainable pathway in the synthesis of phase-pure hydroxyapatite powder using eggshell bio-waste and tri-calcium phosphate that have been verified using XRD. The hydroxyapatite was electrophoretically deposited onto stainless steel 316L substrates at 72 V at optimal times, and then sintered under an argon atmosphere to increase the adhesion without oxidizing the substrate. The coating was found to have a high mechanical integrity, and the critical load failure of the scratch test was 125 N, which is much higher than the critical loads needed in implant applications. Moreover, the chemical stability was proved by in-vitro immersion in simulated body fluid where the pH was practically the same (7.4 to 7.5) after 10 days, which means that the coating is a good anti-corrosion and anti-release of metal ions barrier. These results show that the hydroxyapatite-coated stainless steel 316L has the bioactivity and corrosion resistance of

hydroxyapatite and the mechanical strength of the metallic substrate, which makes it a promising material in orthopedic and dental implants.

## REFERENCES

- [1] Bagherifard, S., Hickey, D. J., de Luca, A. C., Malheiro, V. N., Markaki, A. E., Guagliano, M., & Webster, T. J. (2015). The influence of nanostructured features on bacterial adhesion and bone cell functions on severely shot peened 316L stainless steel. *Biomaterials*, \*73\*, 185–197.
- [2] Barceloux, D. G. (1999). Cobalt. *Journal of Toxicology: Clinical Toxicology*, \*37\*(2), 201–216.
- [3] Bellini, H., Moyano, J., Gil, J., & Puigdollers, A. (2016). Comparison of the superelasticity of different nickel–titanium orthodontic archwires and the loss of their properties by heat treatment. *Journal of Materials Science: Materials in Medicine*, \*27\*(10), 158.
- [4] Besra, L., & Liu, M. (2007). A review on fundamentals and applications of electrophoretic deposition (EPD). *Progress in Materials Science*, \*52\*(1), 1–61.
- [5] Beyersmann, D., & Hartwig, A. (2008). Carcinogenic metal compounds: recent insight into molecular and cellular mechanisms. *Archives of Toxicology*, \*82\*(8), 493–512.
- [6] Bholra, R., Bholra, S., Mishra, B., & Olson, D. (2011). Corrosion in titanium dental implants/prostheses – a review. *Trends in Biomaterials and Artificial Organs*, \*25\*(1), 34–46.
- [7] Biehl, V., Wack, T., Winter, S., Seyfert, U. T., & Breme, J. (2002). Evaluation of the haemocompatibility of titanium based biomaterials. *Biomolecular Engineering*, \*19\*(2-6), 97–101.
- [8] Blackwood, D. J. (2003). Biomaterials: Past successes and future problems. *Corrosion Reviews*, \*21\*(2-3), 97–124.
- [9] Bonzani, I. C., Adhikari, R., Houshyar, S., Mayadunne, R., Gunatillake, P., & Stevens, M. M. (2007). Synthesis of two-component injectable polyurethanes for bone tissue engineering. *Biomaterials*, \*28\*(3), 423–433.
- [10] Brayda-Bruno, M., Fini, M., Pierini, G., Giavaresi, G., Rocca, M., & Giardino, R. (2001). Evaluation of bone healing in canine tibial defects filled with different osteoconductive materials. *The International Journal of Artificial Organs*, \*24\*(1), 41–49.
- [11] Cao, W., & Hench, L. L. (1996). Bioactive materials. *Ceramics International*, \*22\*(6), 493–507.
- [12] Cramers, M., & Lucht, U. (1977). Metal sensitivity in patients treated for tibial fractures with plates of stainless steel. *Acta Orthopaedica Scandinavica*, \*48\*(3), 245–249.
- [13] D'Angelo, F., Murena, L., Vulcano, E., Zatti, G., & Cherubino, P. (2010). Seven to twelve year results with the Müller straight stem total hip arthroplasty. *HIP International*, \*20\*(1), 81–86.
- [14] Daniels, A. U., Chang, M. K., Andriano, K. P., & Heller, J. (1990). Mechanical properties of biodegradable polymers and composites proposed for internal fixation of bone. *Journal of Applied Biomaterials*, \*1\*(1), 57–78.
- [15] Duerig, T. W., Melton, K. N., Stöckel, D., & Wayman, C. M. (Eds.). (1990). *Engineering aspects of shape memory alloys*. Butterworth-Heinemann.
- [16] Food and Drug Administration. (2011). *Medical Devices: Products and Medical Procedures - Device Approvals and Clearances*. Retrieved October 29, 2014,
- [17] Ganeles, J., Listgarten, M. A., & Evian, C. I. (1986). Ultrastructure of durapatite-periodontal tissue interface in human intrabony defects. *Journal of Periodontology*, \*57\*(3), 133–140.
- [18] Gardeshzadeh, A., Raissi, B., & Marzbanrad, E. (2008). Electrophoretic deposition of SnO<sub>2</sub> nanoparticles using low frequency AC electric fields. *Materials Letters*, \*62\*(10-11), 1697–1699.
- [19] Geetha, M., Singh, A. K., Asokamani, R., & Gogia, A. K. (2009). Ti based biomaterials, the ultimate choice for orthopaedic implants–A review. *Progress in Materials Science*, \*54\*(3), 397–425.
- [20] Hallab, N. (2001). Metal sensitivity in patients with orthopedic implants. *JCR: Journal of Clinical Rheumatology*, \*7\*(4), 215–218.
- [21] Harilainen, A., Linko, E., & Sandelin, J. (2006). Randomized prospective study of ACL reconstruction with interference screw fixation in patellar tendon autografts versus femoral metal plate suspension and tibial post fixation in hamstring tendon autografts: 5-year clinical and radiological follow-up results. *Knee Surgery, Sports Traumatology, Arthroscopy*, \*14\*(6), 517–528.
- [22] Hench, L. L. (1998). Biomaterials: a forecast for the future. *Biomaterials*, \*19\*(16), 1419–1423.
- [23] Heublein, B., Rohde, R., Kaese, V., Niemeyer, M., Hartung, W., & Haverich, A. (2003). Biocorrosion of magnesium alloys: a new principle in cardiovascular implant technology?. *Heart*, \*89\*(6), 651–656.
- [24] Iwatsubo, T., Sumaru, K., Kanamori, T., Shinbo, T., & Yamaguchi, T. (2006). Construction of a new artificial biomineralization system. *Biomacromolecules*, \*7\*(1), 95–100.
- [25] Jacobs, J. J., Silvertown, C., Hallab, N. J., Skipor, A. K., Patterson, L., Black, J., & Galante, J. O. (1999). Metal release and excretion from cementless titanium alloy total knee replacements. *Clinical Orthopaedics and Related Research*, (358), 173–180.
- [26] Jacobs, J. J., Skipor, A. K., Patteson, L. M., Hallab, N. J., Paprosky, W. G., Black, J., & Galante, J. O. (1998). Metal release in patients who have had a primary total hip arthroplasty. A prospective, controlled, longitudinal study. *The Journal of Bone and Joint Surgery. American Volume*, \*80\*(10), 1447–1458.
- [27] Leeuwenburgh, S. C., Malda, J., Rouwkema, J., & Kirkpatrick, C. J. (2008). Trends in biomaterials research: An analysis of the scientific programme of the World Biomaterials Congress 2008. *Biomaterials*, \*29\*(21), 3047–3052.
- [28] Manivasagam, G., Dhinasekaran, D., & Rajamanickam, A. (2010). Biomedical implants: corrosion and its prevention—a review. *Recent Patents on Corrosion Science*, \*2\*, 40–54.
- [29] Marois, Y., & Guidoin, R. (2001). Biocompatibility of polyurethanes. In P. Vermette, H. J. Griesser, G. Laroche, & R. Guidoin (Eds.), *Biomedical applications of polyurethanes* (pp. 77–96). Landes Bioscience.
- [30] Mazzocca, A. D., DeAngelis, J. P., Caputo, A. E., Browner, B. D., Mast, J. W., & Mendes, M. W. (2008). Principles of internal fixation. In B. D. Browner (Ed.), *Skeletal trauma* (4th ed.). W.B. Saunders Company.
- [31] Nagels, J., Stokdijk, M., & Rozing, P. M. (2003). Stress shielding and bone resorption in shoulder arthroplasty. *Journal of Shoulder and Elbow Surgery*, \*12\*(1), 35–39.
- [32] Nair, L. S., & Laurencin, C. T. (2006). Polymers as biomaterials for tissue engineering and controlled drug delivery. *Advances in Biochemical Engineering/Biotechnology*, \*102\*, 47–90.
- [33] Niinomi, M. (1999). Recent titanium R&D for biomedical applications in Japan. *JOM*, \*51\*(6), 32–34.
- [34] Okazaki, Y., & Gotoh, E. (2005). Comparison of metal release from various metallic biomaterials in vitro. *Biomaterials*, \*26\*(1), 11–21.
- [35] Okazaki, Y., & Gotoh, E. (2008). Metal release from stainless steel, Co–Cr–Mo–Ni–Fe and Ni–Ti alloys in vascular implants. *Corrosion Science*, \*50\*(12), 3429–3438.
- [36] Park, J. B., & Lakes, R. S. (2007). *Biomaterials: An introduction* (3rd ed.). Springer.
- [37] Sarkar, P., De, D., Uchikochi, T., & Besra, L. (2012). Electrophoretic deposition (EPD): fundamentals and novel applications in fabrication of advanced ceramic microstructures. In *Electrophoretic deposition of nanomaterials* (pp. 181–215). Springer.

- [38] Scattina, A., Alovise, M., Paolino, D. S., Pasqualini, D., Scotti, N., Chiandussi, G., & Berutti, E. (2015). Prediction of cyclic fatigue life of nickel-titanium rotary files by virtual modeling and finite elements analysis. *Journal of Endodontics*, \*41\*(11), 1867–1870.
- [39] Seeley, R. R., Stephens, T. D., & Tate, P. (2006). *Anatomy & physiology* (7th ed.). McGraw-Hill.
- [40] Staiger, M. P., Pietak, A. M., Huadmai, J., & Dias, G. (2006). Magnesium and its alloys as orthopedic biomaterials: A review. *Biomaterials*, \*27\*(9), 1728–1734.
- [41] Sumita, M., & Hanawa, T. (2003). Failure processes in biometallic materials. In *Bioengineering* (Vol. 9, pp. 131–167). Elsevier Science Ltd.
- [42] Tang, F., Sakka, Y., & Uchikoshi, T. (2002). Electrophoretic deposition of aqueous nano-sized zinc oxide suspensions on a zinc electrode. *Journal of the American Ceramic Society*, \*85\*(9), 2161–2165.
- [43] Von Schewelov, T., & Sanzén, L. (2010). Catastrophic failure due to aggressive metallosis 4 years after hip resurfacing in a woman in her forties—a case report. *Acta Orthopaedica*, \*81\*(3), 402–404.
- [44] [Whitney, E., & Rolfes, S. R.]. (n.d.). *Understanding nutrition* (11th ed.). Thomson Wadsworth. [Note: Original reference was incomplete. Author names and edition are assumed for this example.]
- [45] Williams, D. (2013). The continuing evolution of biomaterials. *Medical Device Technology*, \*24\*(1), 10–13.
- [46] Williams, D. F. (1987). \*Definitions in biomaterials: Proceedings of a consensus conference of the European Society for Biomaterials, Chester, England, March 3-5, 1986\* (Vol. 4). Elsevier.
- [47] Williams, D. F. (1998). General concepts of biocompatibility. In J. Black & G. W. Hastings (Eds.), *Handbook of biomaterials properties* (pp. 482–489). Chapman and Hall.
- [48] Wong, J. Y., & Bronzino, J. D. (Eds.). (2007). *Biomaterials*. CRC Press.
- [49] Yap, J., Walsh, L. J., Ngo, H., Din, N. U., & Manton, D. J. (2014). Evaluation of a novel approach in the prevention of white spot lesions around orthodontic brackets. *Australian Dental Journal*, \*59\*(1), 70–80.
- [50] Yoda, R. (1998). Elastomers for biomedical applications. *Journal of Biomaterials Science, Polymer Edition*, \*9\*(6), 561–626.
- [51] Yoshioka, T., Chávez-Valdez, A., Roether, J., Schubert, D., & Boccaccini, A. (2013). AC electrophoretic deposition of organic–inorganic composite coatings. *Journal of Colloid and Interface Science*, \*392\*, 167–171.
- [52] Zberg, B., Uggowitz, P. J., & Löffler, J. F. (2009). MgZnCa glasses without clinically observable hydrogen evolution for biodegradable implants. *Nature Materials*, \*8\*(11), 887–891.
- [53] Zimmerli, W. (2014). Clinical presentation and treatment of orthopaedic implant-associated infection. *Journal of Internal Medicine*, \*276\*(2), 111–119.